CHALMERS

Design of a beam switch for the mm-wave receiver at Onsala Space Observatory

Design av beam switch till mm-vågsmottagare för Onsala rymdobservatorium
Examensarbete inom högskoleingenjörsprogrammet Mekatronikingenjör

CHRISTIAN OLSSON

Department of Earth and Space Sciences
CHALMERS UNIVERSITY OF TECHNOLOGY
Gothenburg, Sweden 2011

Design of a beam switch for the mm-wave receiver at Onsala Space Observatory

Christian Olsson

THESIS FOR THE DEGREE OF BACHELOR OF SCIENCE IN ENGINEERING

Group for Advanced Receiver Development
Onsala Space Observatory
Department for Earth and Space Sciences

CHALMERS UNIVERSITY OF TECHNOLOGY
Gothenburg, Sweden 2011

Design of a beam switch for the mm-wave receiver at Onsala Space Observatory
CHRISTIAN OLSSON

The work was conducted at:
Group for Advanced Receiver Development,
Onsala Space Observatory
Department of Earth and Space Sciences

Chalmers University of Technology,
Kemivägen 9
SE-412 96 Gothenburg, Sweden
Telephone + 46 (0)31 772 1806
Fax: +46 (0)31 772 1801
Email: colsson@student.chalmers.se

Cover:
Onsala Space Observatory.
Night photo of the 20-meter telescope radome enclosure. The antenna and receiver for radio astronomy millimetre waves are mounted on a position control system inside the radome.
Photo: Jan-Olof Yxell

Printed:
Department of Earth and Space Sciences
Chalmers University of Technology
Gothenburg, Sweden 2011

Design of a beam switch for the mm-wave receiver at Onsala Space Observatory
CHRISTIAN OLSSON
Department for Earth and Space Sciences
Onsala Space Observatory
Chalmers University of Technology

Abstract

Ground-based astronomical observations at millimetre wavelengths are very challenging due to the strong influence of the rapidly fluctuating water content in the Earth's atmosphere. Calibration to compensate for atmospheric disturbances and also to the receiver's limited stability is done by switching rapidly between the source under observation and cold space. Prior to the upgrade of the 3 mm wavelength receiver at Onsala Space Observatory an evaluation of different designs of the beam switch is needed.

The work was done at the Group for Advanced Receiver Development (GARD) at the department for Earth and Space Sciences at Chalmers University of Technology. GARD develops receivers for mm- and submillimetre waves used for radio astronomy and environmental sciences.

Five different switching methods have been evaluated and one of them has been analyzed in detail. A 3D model was made in the CAD system Autodesk Inventor and the mechanical analysis of different structural deformation was carried out in ANSYS.

The simulations carried out in ANSYS were, static structural directional deformation during acceleration, transient structural directional deformation during acceleration, modal analysis and static structural stress equivalent (von-Mises). The results confirmed that there were very small deformations and vibrations in the direction normal to the mirror plane. Further, the results showed that the Self-Resonant Frequency (SRF) is well above the frequency of the mechanical movement and it can be concluded that there is no risk for oscillations. The structural stress analysis also showed that the material used in the design, an aluminium alloy, is an appropriate choice for the application.

Drive units for the beam switch were evaluated and partly analyzed. Different alternatives for the drives can be electrical motor or pneumatic actuator. A possible solution to obtain a smooth operation, i.e. smooth change in direction of the mirror, is to employ a crankshaft mechanism.

Critical parts of the system that have to be further evaluated through testing are the tolerances for the guideways and limits in speed and lifetime for the pneumatic actuators.

Sections that will not be dealt with are the climate impact on the design, which consists of variations in temperature and humidity, the energy consumption and systems environmental impact on nature.

Acknowledgements

After an interesting journey in the world of studies including physics, electronics, digital technology, programming, chemistry, economics, and not at least mathematics it goes to the finals with this graduation report for Bachelor of Science degree in Mechatronics Engineering at Chalmers University of Technology. My previous practical experience has been supplemented by theoretical knowledge that will be very handy in the future.

I would like to thank the Department of Earth and Space Sciences, and my examiner and head of GARD, Professor Victor Belitsky for his permission to carry out this thesis.

I offer my sincerest gratitude to my two supervisors, Lic. Eng. E.E. Olle Nyström, who has supported me throughout my thesis with his expertise and knowledge. And Research Engineer Mathias Fredrixon for his time, knowledge and patience during deep discussions of intricate problems.

Igor Lapkin for technical information and explanations, Magnus Strandberg for support during simulations with ANSYS and Alexey Pavolotsky for his expert knowledge. In my daily work I have been blessed with the friendly and cheerful group GARD, thank you all.

Table of Contents

CHAPTER 1

INTRODUCTION

The Group for Advanced Receiver Development (GARD) develops receivers for millimetre and sub-millimetre waves used in Radio Astronomy and Environment Science [1]. GARD is an instrumentation group of Onsala Space Observatory (OSO) [2].

1.1. Background

The Onsala Space Observatory, located at the Onsala peninsula 45 km south of Gothenburg, is the Swedish National Facility for Radio Astronomy. The observatory has two radio telescopes, a 20-meter and a 25-meter telescope, providing the scientists the possibilities to study the stellar birth and death, by the molecular spectroscopy method in the Milky Way and other galaxies. The research group GARD is currently designing a new receiver for the 3mm and 4mm wavelength band. The receiver will be situated in the Cassegrain cabin of the 20-meter telescope. Ground-based astronomical observations at millimetre wavelengths are very challenging due to the strong influence of the Earths' atmosphere which has to be accounted for during observations. The signal levels in radio astronomy is extremely weak, substantially less that the noise level, which accompanies the signal. Typically signal levels ranges from 30 to 300 times less then that radiated by objects at room temperature, according Rayleigh and Jeans law. Quite often long-time integration is required to get sufficient signal-to-noise ratio. During the integration procedure, the extremely weak signal that is to be detected is affected by interference due to the rapidly fluctuating water content in the Earth's atmosphere and instability of the receiver transmission coefficient.

In order to exploit the receiver's maximum sensitivity and achieve optimum signal-to-noise ratio, it is necessary to calibrate for these disturbances. Calibration to compensate for atmospheric disturbances and also to the receiver's limited stability is done by switching rapidly between the observation object and cold background observation, i.e. on the side of the object where the telescope is looking, toward the cold space. For compensation of the atmospheric instability, the switching period should be less than 1 sec. The telescope has significant momentum and could not switch with the required time period. To provide fast switching, a beam switching based on a mechanically manipulated mirror, that redirect the beam between two mirrors situated with offsets in the focal plane, is used. This provides proper beam separation on sky.

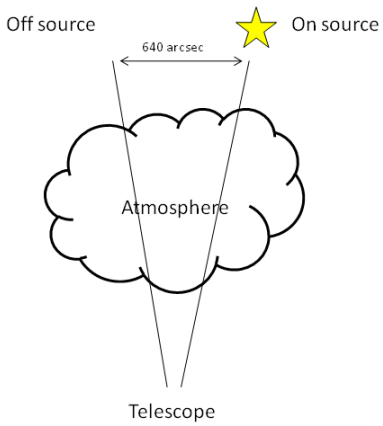

Figure 1.1-1 Switching on/off-source.

Switching between the directions of the antenna lobe is done by a mirror tilted in different positions by means of an electric motor, which itself is a potential source of instability for the extremely sensitive receivers. During the switching cycle on/off-source, the mirror will, for a short transition time period, be at a position where neither the source signal nor the calibration signal can be measured. In result some part of the integration time is lost and this degrades the receiver sensitivity. This "parasitic" part of the switching cycle must be minimized not to lose precious observing time.

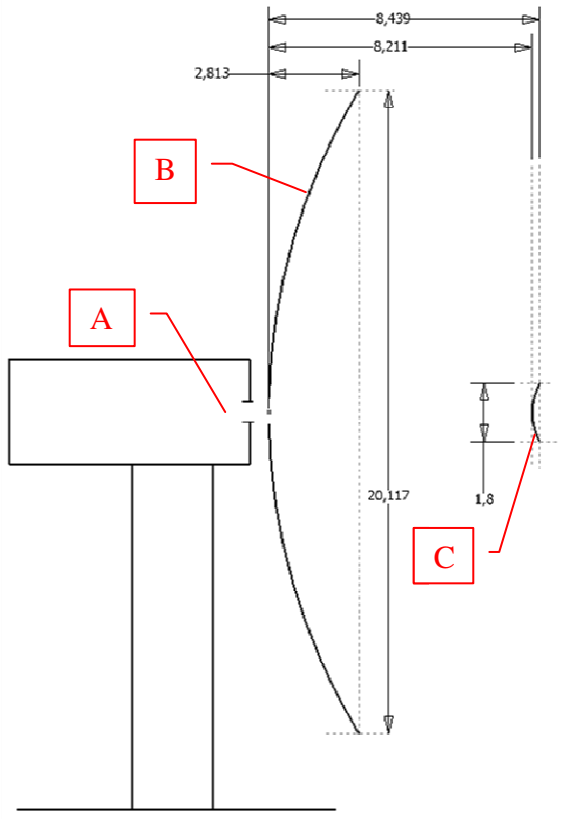

Figure 1.1-2 Schematic picture of radio telescope, A Cabin, B primary reflector, C sub-reflector. All dimensions in metre.

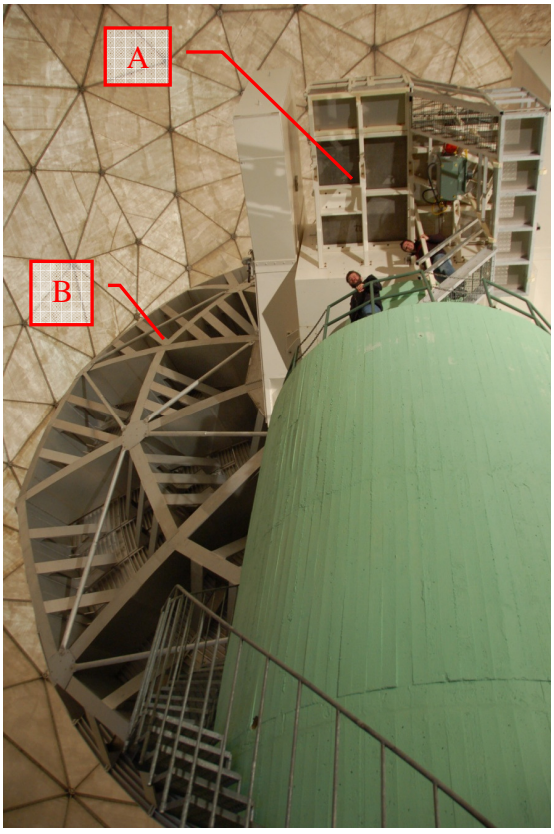

Figure 1.1-3 Antenna and Cabin of the Onsala 20-metre telescope inside the radome enclosure. A Cabin, B primary reflector.

With a flipping mirror it is only possible to use a single receiver. With a mirror that moves in and out of the beam it is possible to use a dual receiver with two different channels. The mirror market in red is the flipping mirror. A turning movement is carried out around its own axis.

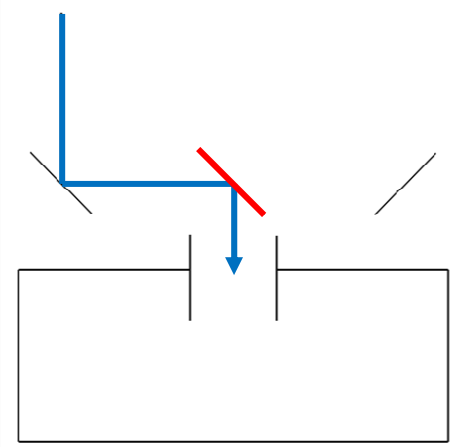

Figure 1.1-4 Single receiver with flipping mirror marked in red. First path way.

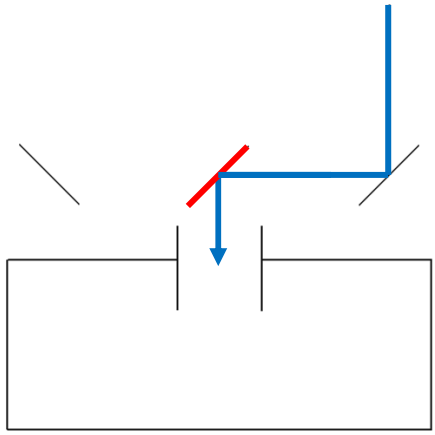

Figure 1.1-5 Single receiver with flipping mirror marked in red. Second path way.

With a sliding mirror there are always two path ways to the receiver. Sliding mirror is shown in green.

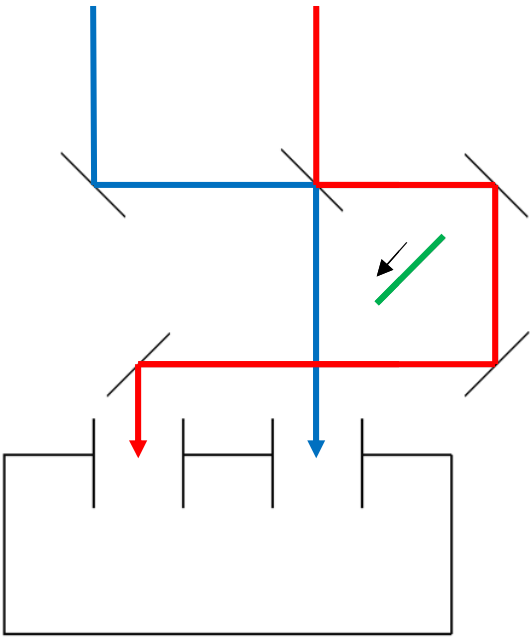

Figure 1.1-6 Dual receiver with sliding mirror marked in green. First path ways.

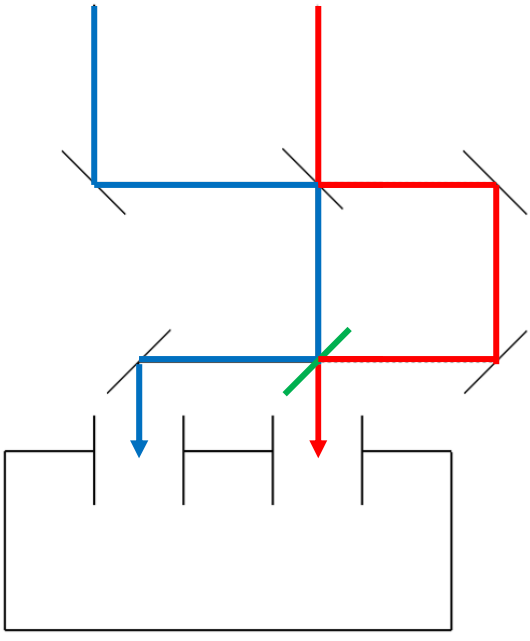

Figure 1.1-7 Dual receiver with sliding mirror marked in green. Second path ways.

1.2. Purpose

Prior to the upgrade of the receiver an evaluation is needed of different solutions to the so-called "beam switch". The evaluation should consider mirror deformations, vibrations, transition time (blanking time), size and reliability estimation. Various mechanical solutions of the movement or rotation of the mirror will be evaluated against each other. Focus will be on a sliding mirror solution. It is a new solution that has not previously been examined in Onsala.

1.3. Delimitations

Sections that will not be dealt with are the climate impact on the design, which consists of variations in temperature and humidity. Climate impact is neglected due to the climate controlled environment inside the cabin where the receiver is installed. Environmental effects that otherwise should have been considered are material effects e.g. corrosivity. Other delimitations in the work are energy consumption and the systems environmental impact on nature.

1.4. Requirements

To ensure the bean switch function, there are certain specifications that should be met. Some specifications are unchanged because they belong to the technical function, others are set with regard of being improved or at least as good as the previous installation.

- Total beam switching cycle shall be one second
- Max blanking time shall not exceed 100ms
- Observing time, on/off source, shall not be less than 800ms.
- Max angular beam deviation due to misalignment of the mirror shall be 490 arcseconds
- Mirror repeatability during operation shall be 1 arcsecond
- Total operating time must be longer than six months (1,536,000 repetitions) before service is needed

1.5. Project goals

Designing beam switch for the new Onsala Space Observatory mm-wave receiver will include the following steps.

- Evaluate different switching methods for the mirror beam switch
- Analyse the sliding mirror solution
- Evaluate which geometry and tolerances are important to the guideways and the effect on the beam
- Evaluate different mechanical drives for the system (electric motor, crankshaft mechanism and pneumatics)
- CAD of the system, 3D model
- Mechanical analysis in ANSYS for deformation and stress. Static structural directional deformation during acceleration, transient structural directional deformation during acceleration, modal analysis and static structural stress equivalent (von-Mises) [3]
- Suggestions for future work

CHAPTER 2

THEORY

This chapter deals with formulas necessary for analyses of trigonometry, mechanics and fluid mechanics, using the following references [4], [5], [6].

2.1. Angular relations

An angular displacement of the mirror will result in double faults in outgoing beam, shown in Figure 2.1-1 and 2.1-2. Mirror is shown in red and beam in black.

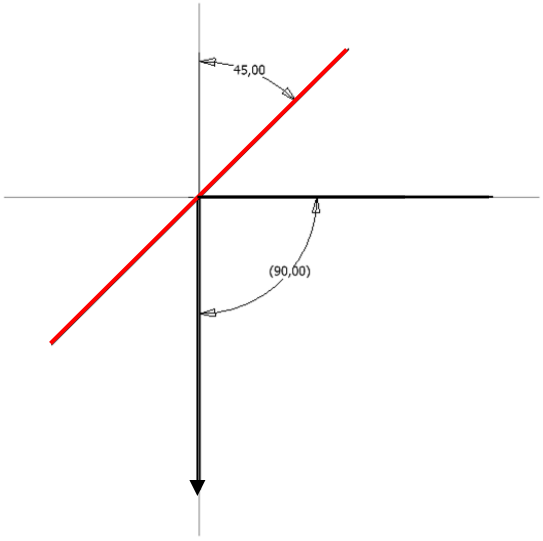

Figure 2.1-1 45°mirror and 90°beam

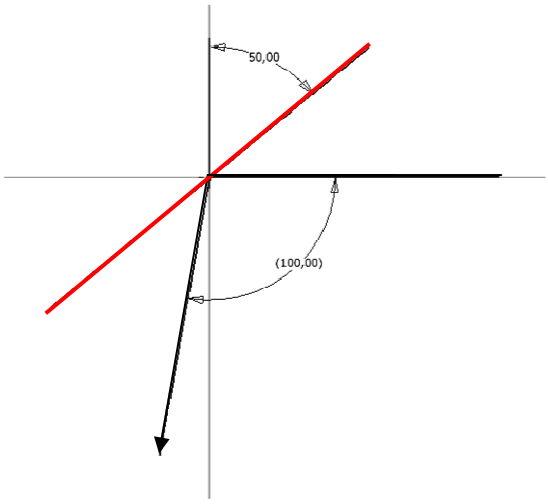

Figure 2.1-2 50°mirror and 100°beam

Arcseconds are commonly used in astronomy as a measure of angles. One arcsecond is 1 / 3600 degree, in comparison, an object, 1 mm in diameter, observed at a distance of 206 m would have an opening angle of 1 arcsecond.

2.2. Mechanics

When the beam switch is set in motion from stationary state, acceleration a occurs. It can be solved from final velocity v, initial velocity v_0 and time t

$$a = \frac{v - v_0}{t} \tag{2.1}$$

Final velocity v during uniform acceleration is calculated from length L, and time t

$$v = \frac{2L}{t} \tag{2.2}$$

Acceleration is calculated if final velocity is unknown with, equations 2.2 inserted in 2.1.

$$a = \frac{2(L - v_0 t)}{t^2} \tag{2.3}$$

The force F needed for the desired acceleration a can be solved if mass m is known with Newton's Second law of motion

$$F = ma \tag{2.4}$$

2.3. Fluid Mechanics, Flow Work

Force obtained from pneumatic actuators as a result of area and pressure, gas consumption as a result of number of repetitions, pressure and volume is solved by the following formulas.

2.3.1. Force

The force *F* from a pneumatic actuator is obtained from the pressure *P* that is supplied and the area *A* of the piston.

$$F = PA \tag{2.5}$$

$$1\ N/m^2 = 1\ Pa \tag{2.6}$$

The pressure is often measured in bars, but correct notation according to the SI system *(**S**ystème **i**nternational d'unités)* is in the unit pascal $[Pa]$.

$$1\ bar = 100\ kPa \tag{2.7}$$

2.3.2. Gas consumption

To determine the gas consumption of a pneumatic actuator the atmospheric air volume flow rate $\dot{\mathcal{V}}_{atm}$ is solved with the following formulas.

$$P\mathcal{V} = mRT \quad \text{, the ideal gas law} \tag{2.8}$$

The air mass m in the pneumatic actuators volume $\mathcal{V}_{cyl}$ under supplied air pressure P_{sup} is calculated with

$$m = \frac{P_{sup}\mathcal{V}_{cyl}}{RT} \tag{2.9}$$

The gas constant *R* for air is 287 $J/kg \cdot K$, and room temperature *T* is 294,15 *K*.

The mass makes it possible to calculate the free air volume $\mathcal{V}_{atm}$. Compressor performance is commonly measured by free air delivery in liters per minute resulting in

$$\mathcal{V}_{atm} = \frac{mRT}{P_{atm}} \quad ,1\ atm = 101.325\ kPa \tag{2.10}$$

and the atmospheric air volume flow rate is given by:

$$\dot{\mathcal{V}}_{atm} = n\mathcal{V}_{atm} \quad \text{, } n \text{ is the number of strokes per second} \tag{2.11}$$

where

$$1\ m^3/s = 60\ 000\ L/min \tag{2.12}$$

CHAPTER 3

METHOD

The work is planned in order to complete the CAD of the mirror movement mechanism in Autodesk Inventor [7], the development of the design drawings, and an introduction to ANSYS in parallel with the literature survey, selection of beam switching method and choice of guiding- and drive system.

3.1. Mechanical design

Choice of beam switching method will be selected with the aim for as short switching time as possible while maintaining a stable and vibration free operation.

Choice of mechanical guiding system for positioning of the mirror will be selected for smooth and precise (repeatable) movement. The moving mass of the guiding system is also vital to the function. A large mass creates vibrations and deformations in the structure during acceleration and deceleration, and increases the wear on mechanical parts. Service intervals on the mechanism are also an issue to be considered and should not be less than half a year not to interfere with the measurements and observations.

Choice of drive system will be selected for force and speed and the possibility of the mirror position to be controlled. The risk of electric and magnetic interference on the receiver has to be considered.

3.2. Analysis of the mechanism

In order to evaluate the beam switch in terms of deformation and vibrations extensive simulations with the Finite Element Method (FEM) is performed with the commercial software ANSYS. The simulations include static structural directional deformation during acceleration, transient structural directional deformation during acceleration, modal analysis, static structural stress equivalent (von-Mises).

3.3. Evaluation

The evaluation will include the results of ANSYS-simulations and propose appropriate solutions and recommendations for future work.

CHAPTER 4

DIFFERENT BEAM SWITCHING METHODS

4.1. Current method

This chapter begins with a description of the mechanism of the currently existing beam switch, installed in the Onsala observatory in 1984, where the advantages and disadvantages are discussed.

4.1.1. Electro-Mechanical Flipping Mirror

Current method uses an electric motor. The motor is connected via a belt drive transmission to a gearbox. The gear box contains the mechanism that moves the mirror which is lubricated in an oil bath. The mirror is positioned below the gearbox and is exposed to the risk of oil leakage which could contaminate the mirror. There is also a certain wear of the mechanical guidance system which is undesirable. The turning movement of the mirror is carried out around its own axis. An advantage of this type of switching is the inherent symmetry of the switching where additional folding mirrors, to couple the beam to the sub-reflector, can be placed symmetrically around the switch and thus easily keep the same signal path length to the sub-reflector. Disadvantages, apart from the ones stated above, is that this solution is suitable for one receiving beam only and the mirror is prone to vibration in its' end positions (when the mirror stops) resulting in a longer blanking time, since a delay has to be implemented in the measurements for the vibrations to decay.

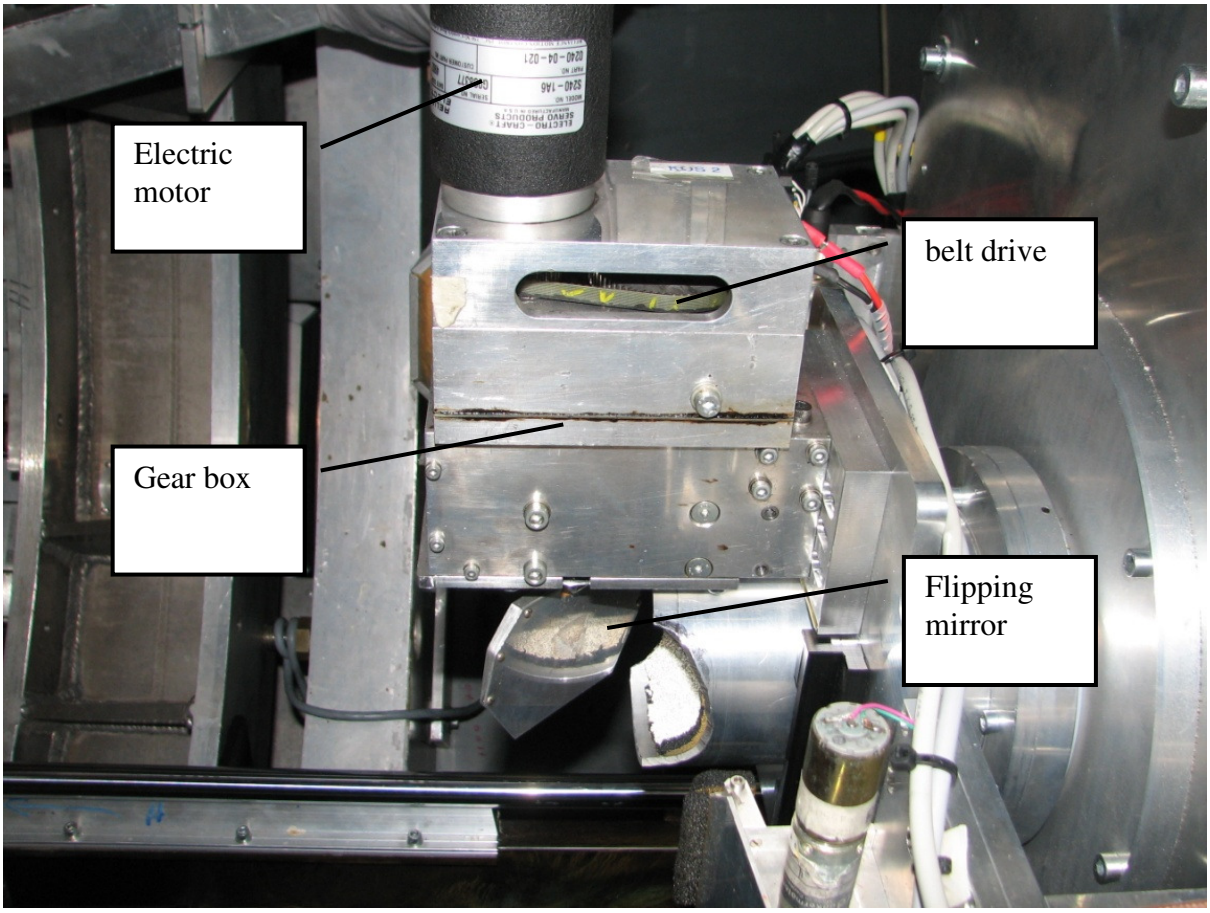

Figure 4.1.1-1 Current beam switch at Onsala Space Observatory (OSO) mm-wave receiver

4.2. Alternative methods

Following are some alternative methods that exist or are under development. The mechanism's function is described and each one's pros and cons.

4.2.1. Chopper Wheel

Chopper wheel is a circular disk that consists of two or more sections. Either the beam is reflected on the side of the wheel or goes straight through it. The wheel needs to be large in order to allow “long” time when the beam is on/off source and keeping the transition time short, i.e. to minimize the blanking time. Something which affects the wheel size also is the beam width. The required big size is the main disadvantage of this switching mechanism, especially in the case for a two channel receiver where the available space on top of the cryostat will be very limited. The advantage is that the movement is relatively steady and stable. This method requires few moving parts, only the wheel is spinning.

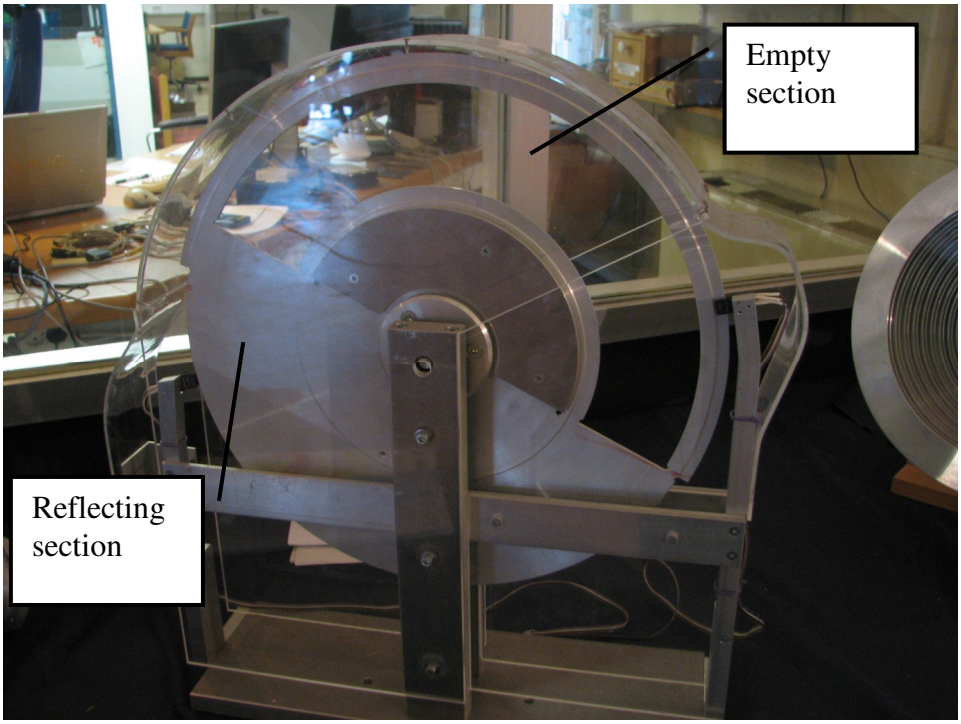

Figure 4.2.1-1 Chopper wheel display model at Onsala Space Observatory.

4.2.2. Pneumatic Flipping Mirror

A pneumatic rotary actuator with adjustable stops is used for the turning movement. The air supply is controlled by two solenoid actuators and the turning movement of the mirror is carried out around its own axis. The advantages are the same as for the electro-mechanical switch with its' inherent symmetry. The disadvantage is that shorter blanking time brings more vibrations due to the fast deceleration of the mass. A feasibility study of this type of switch is currently ongoing at the observatory in Onsala. A disadvantage is that shorter blanking time brings more vibrations due to the fast deceleration of the mass. Figure 4.2.2-1 below [8].

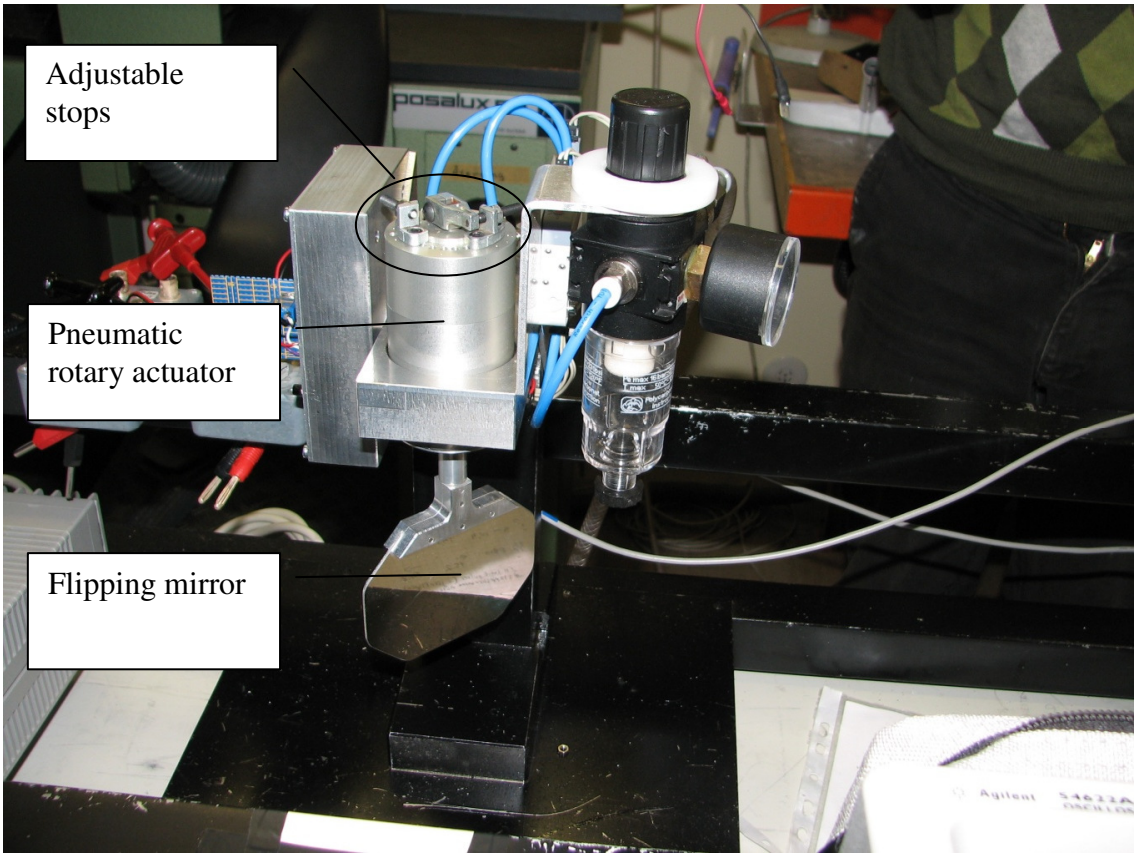

Figure 4.2.2-1 Experimental setup at Onsala Space Observatory. Designed by Per Björklund [8].

4.2.3. Sliding Mirror

The Sliding Mirror moves in its own plane instead of its own axis. This means that it is not sensitive to movements from starting and stopping made in the switching direction. The movement can be optimized by deceleration close to the end positions, reverse its' direction, and have the highest speed at the transition point. With this configuration the on/off positions will be longer and the transition period will be minimized. This also makes it possible to make use of the reflective surface of the mirror, i.e. on-source, while the mirror is in motion. This leads to short blanking times. One drawback is that the design contains several mechanical parts.

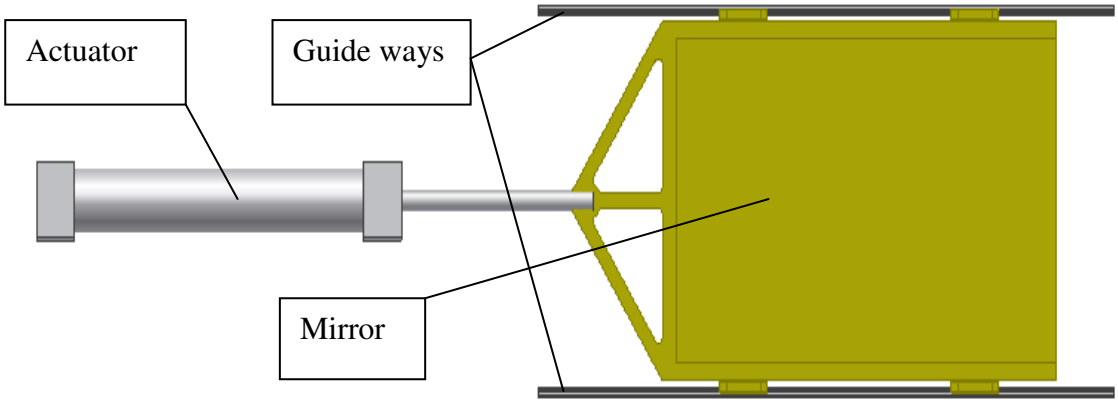

Figure 4.2.3-1 schematic picture of the sliding mirror solution

4.2.4. Adjustable Sub-Reflector

The entire sub-reflector is moved to change the beam path. It is a large, 1.8m in diameter, convex reflector placed in front of the primary 20m-reflector. The relatively large mass makes it difficult to position the reflector quickly and precisely, leading to long blanking times. An advantage is that it is possible to use several receivers and getting a symmetric installation with few mirrors. The Sub-Reflector is marked (C) in Figure 1.1-2.

4.3. Comparison of the methods

There are a various types of switching methods, each with its pros and cons. Some are better in a in a certain configuration than others. In table 4.3-1 the benefits are to be found.

Advantages	Electro-Mechanical Flipping Mirror	Chopper Wheel	Pneumatic Flipping Mirror	Sliding Mirror	Adjustable Sub-Reflector
Little or no mass to move or needs to change direction	•	•	•		
No electric motor			•	•	
No advanced transmission, several mechanical parts or risk of oil leakage		•	•		
Possible to get two symmetric beam paths and few mirrors for one receiver	•		•		•
Possible to get two beam paths for two receiver		•		•	•
Small and relatively compact design	•		•		

Table 4.3-1 Method comparison table

CHAPTER 5

EVALUATION OF DIFFERENT SLIDING MIRROR DESIGNS

The critical direction of deformation/vibrations for the switch mirror is in the mirror's normal direction. A deformation in this direction would introduce an additional tilt of the beam resulting in a beam offset from the centre of the sub-reflector, marked (C) in Figure 1.1-2. Deformation and vibrations are unfortunately unavoidable no matter what switching solution one chooses and in general a time delay is introduced for any vibrations to decay. An interesting approach, however, is to design the beam switch in a way where the vibration in the mirror's normal direction is minimized by allowing larger vibrations in the mirror plane, the time delay could possibly be removed and observations could be performed even during this period. The suggested method is described under 4.2.3, Sliding Mirror. To conduct an evaluation of this switching method based on a sliding mirror it has to be analyzed in detail. The following simulations will be made in the next chapter static structural directional deformation during acceleration, transient structural directional deformation during acceleration, modal analysis, static structural stress equivalent (von-Mises).

5.1. Simulations in ANSYS

Using a powerful software program from ANSYS makes it possible to simulate and predict technical data before production. The engineering simulation software is based on the Finite Element Method (FEM). ANSYS Workbench 13.0 includes the following simulation packages. Multiphysics, Structural mechanics, Fluid Dynamics, Explicit Dynamics, Electromagnetics, Simulation Process & Data Management, Academic, High-Performance Computing, Geometry Interfaces and more.

With the mirror mounted in its frame and carriage, see Figure 5.1-1. Mirror flatness is simulated with regard to deformation measured in the direction normal to it's plane (Directional deformation) during acceleration and deceleration of $30 m/s^2$ (approximately 3G). It is deformation normal do the mirror surface that is interesting to simulate since this is the critical direction in terms of optical beam deviations.

From Equation (2.3)

$$a = \frac{2(L - v_0 \cdot t)}{t^2} = \frac{2(0,15)}{0,1^2} = 30\ [m/s^2] \quad (5.1)$$

A comparison between the acceleration a and the Earth's gravity g, 1G = Earth's gravity (9,80665m/s^2)

$$G = \frac{a}{g} = \frac{30}{9,80665} = 3,059 \quad (5.2)$$

The mirror acceleration is three times the Earth's gravity (3G).

During simulation support surfaces are applied to the design. Frictionless supports for sliding surfaces and fixed support for the surface where it is pulled are considered. The first only provides support in one direction, normal to the plane of the surface it's applied to, and the other one has support in all directions to the surface. Note that the supports are assumed perfect and that the real rails are not part of this simulation.

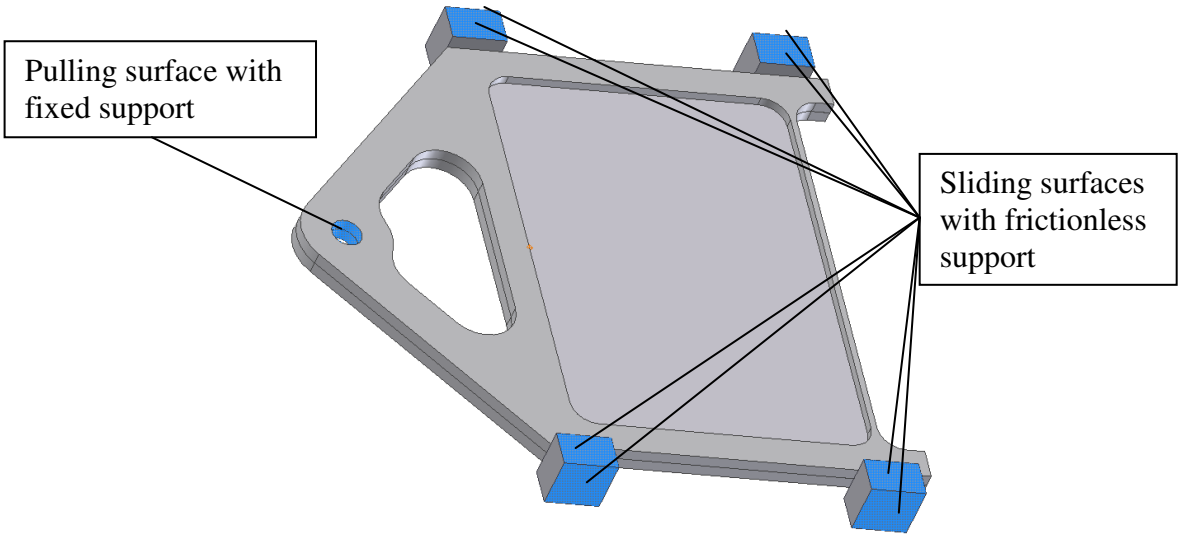

Figure 5.1-1 Carriage with support surface marked in blue

Comparative simulations are made for different materials with the purposes of selection of likely candidates for the final design

Simulations are made with materials for the purposes of a comparative simulation, with mass and materials selected as likely candidates to be implemented in the final design. Selected materials are aluminium, constructional steel and FR-4 for the mirror. In the final solution it will be FR-4 laminated with a thin layer of copper on both sides, in other words a PCB plate. FR-4 is a glass reinforced epoxy laminate made of woven fibreglass cloth with an epoxy resin binder. FR-4 is a specification - not a product in itself [9].

5.1.1. Static structural directional deformation during acceleration

The first simulation is made as simple as possible, Figure 5.1.1-1. The deflection was large around the pulling point which affects the mirror geometry; the reflecting surface is not flat enough anymore. Here and further on, we discuss deformations, which are normal to the mirror plane; measured in mm ($1 \cdot 10^{-6}$ mm = 0.001 µm = 1 nm).

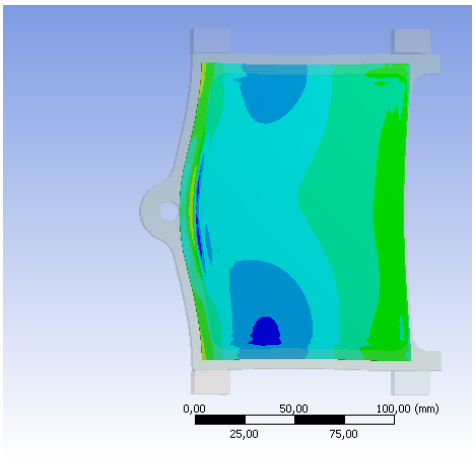

Figure 5.1.1-1 Carriage A-1

$$+\ 0.805\ 110 \cdot 10^{-6}\ mm\ Max$$
$$-\ 0.811\ 970 \cdot 10^{-6}\ mm\ Min$$
$$1.617\ 000 \cdot 10^{-6}\ mm\ Tot$$

A solution to this is to spread the forces on a larger area which reduces the deformation as shown in Figure 5.1.1-2. This also leads to greater weight and have other disadvantages such as large vibration of the whole design. An initial attempt to reduce weight resulted in a weaker design and greater deformation, which is unwanted. The results simulation results are shown in Figure 5.1.1-3.

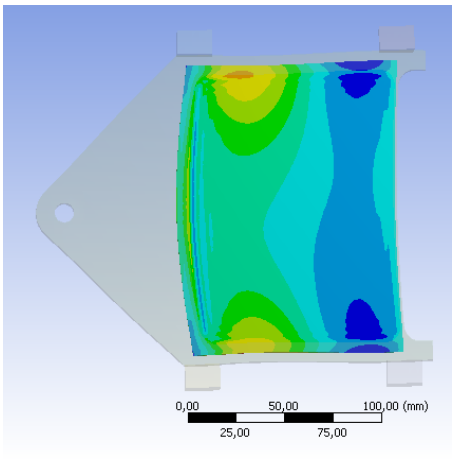

Figure 5.1.1-2 Carriage A-2

$$+\ 0.384\ 310 \cdot 10^{-6}\ mm\ Max$$
$$-\ 0.140\ 420 \cdot 10^{-6}\ mm\ Min$$
$$0.524\ 730 \cdot 10^{-6}\ mm\ Tot$$

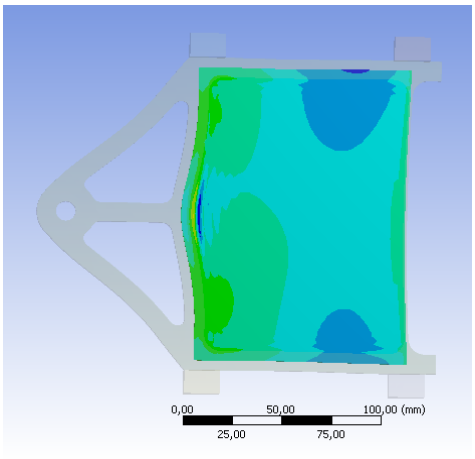

Figure 5.1.1-3 Carriage A-3

$$+\ 0.586\ 260 \cdot 10^{-6}\ Max$$
$$-\ 0.301\ 920 \cdot 10^{-6}\ Min$$
$$0.888\ 000 \cdot 10^{-6}\ Tot$$

After iterative changing of design and simulating with ANSYS software, it was possible to find design (Figure 5.1.1-4 and Figure 5.1.1-5), characterized by the deformation values equivalent to that of carriage A-2 (Figure 5.1.1.2), but sufficiently more light-weight. Note that reversing the direction of the pulling force results in the same total deformation.

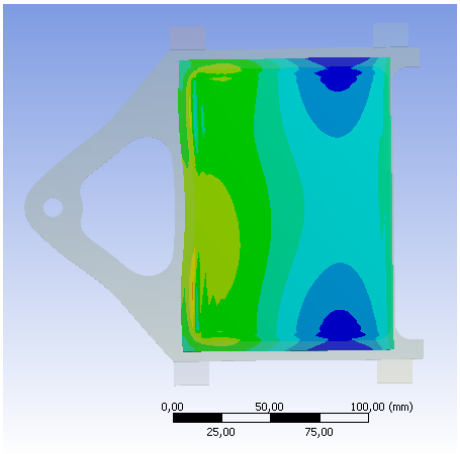

Figure 5.1.1-4 Carriage A-4

$$+\ 0.353\ 240 \cdot 10^{-6}\ mm\ Max$$
$$-\ 0.205\ 060 \cdot 10^{-6}\ mm\ Min$$
$$0.558\ 300 \cdot 10^{-6}\ mm\ Tot$$

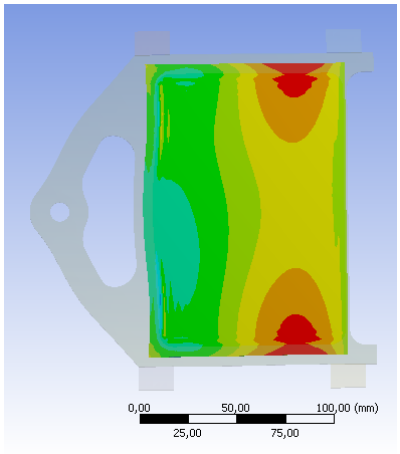

Figure 5.1.1-5 Carriage A-4

$$+\ 0.205\ 060 \cdot 10^{-6}\ mm\ Max$$
$$-\ 0.353\ 240 \cdot 10^{-6}\ mm\ Min$$
$$0.558\ 300 \cdot 10^{-6}\ mm\ Tot$$

Since it was desirable to save space in width between guideways, a narrower solution was developed and tested. Carriage B-2 in Figure 5.1.1-7 is designed so that the pulling is in X direction and through the centre of mass in Y and Z direction. However, increased weight and complexity adds a number of unwanted contributions such as higher mechanical wear, vibrations and deformations. For future work, it should be carefully considered if the gain in space is really worth the additional drawbacks it brings to the system.

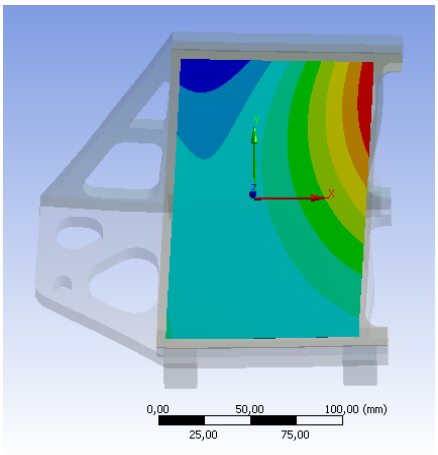

Figure 5.1.1-6 Carriage B-1

$$+\ 113.630 \cdot 10^{-6}\ mm\ Max$$
$$-\ 52.223 \cdot 10^{-6}\ mm\ Min$$
$$165.853 \cdot 10^{-6}\ mm\ Tot$$

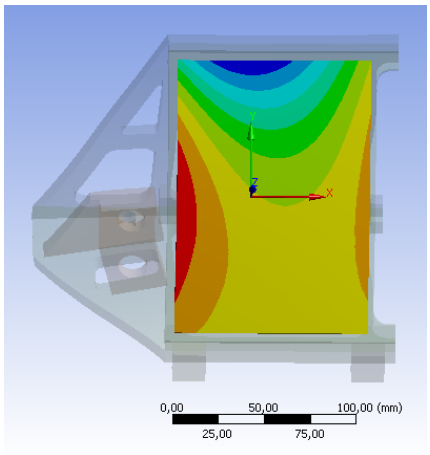

Figure 5.1.1-7 Carriage B-2

$$+\ 36.873 \cdot 10^{-6}\ mm\ Max$$
$$-\ 122.490 \cdot 10^{-6}\ mm\ Min$$
$$159.360 \cdot 10^{-6}\ mm\ Tot$$

5.1.2. Transient structural directional deformation

When the carriage goes from standstill to constant acceleration, vibration is induced. This transient is possible to simulate in ANSYS.In figure 5.1.2-1 the horizontal axis represents time from 0-10ms. The vertical axis represents directional deformation in ±1.25nm. The mirror's highest and lowest points are shown in green and red. After 1.8 ms, a peak of 1.2 nm shows, which is carriage A-4 maximum simulated directional deformation. After 6 ms transients has decayed and only static deformation remains.

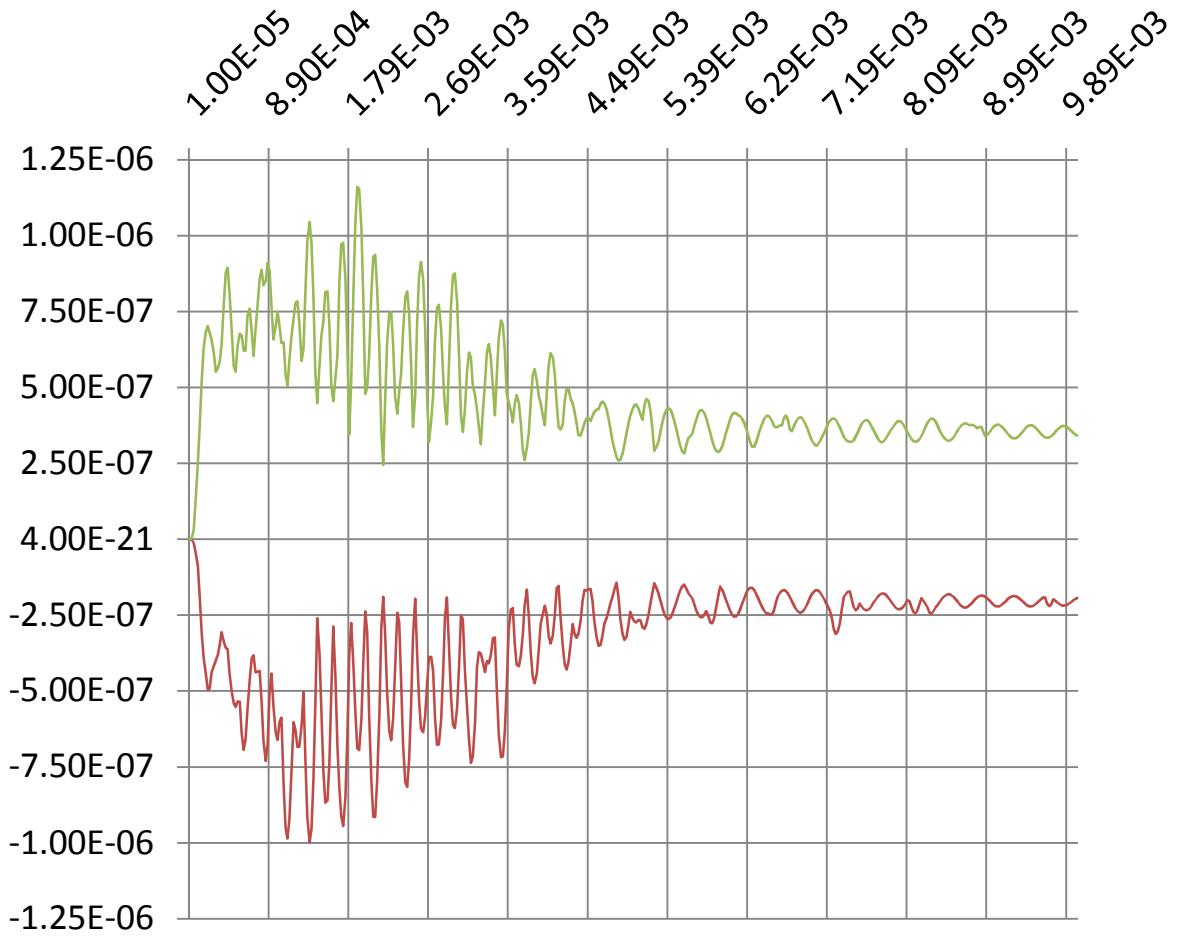

Figure 5.1.2-1 Horizontal axis represents time [s] and vertical axis represents directional deformation [mm] for transient structural directional deformation of Carriage A-4.

Simulated data for carriage B-1 is shown in figure 5.1.2-2. The direction of the deformation is the same as in figure 5.1.2-1 but the time scale in the figure is changed to 0-30 ms and the y-scale (deformation) is ±500 nm. A peak of 500 nm at 2.0 ms shows max directional deformation. Directional deformation of the carriage B-1 is approximately 500 times larger then those for carriage A-4 (figure 5.1.2-1) and lasts sufficiently longer (20ms compared to 6ms).

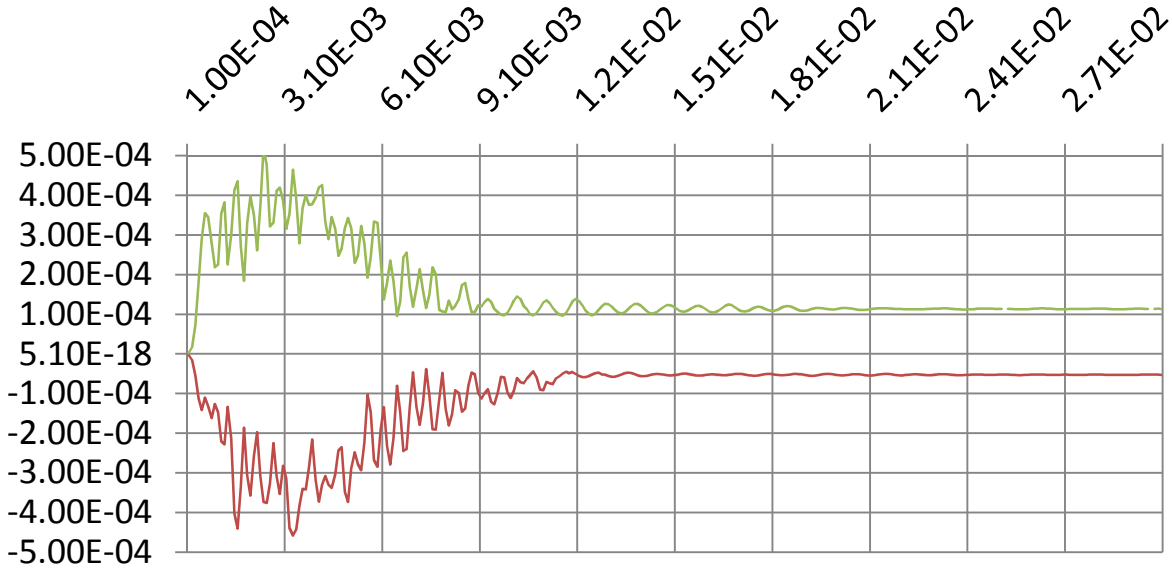

Figure 5.1.2-2 Carriage B-1

As mentioned in chapter 5.5.1 the carriage B-2 is pulled in the centre of mass, which reduces the maximum deformation to 250nm. This should be compared to the simulated results for A-4, exhibiting a deformation of 1.2 nm. Simulated results are shown in figure 5.1.2-1.

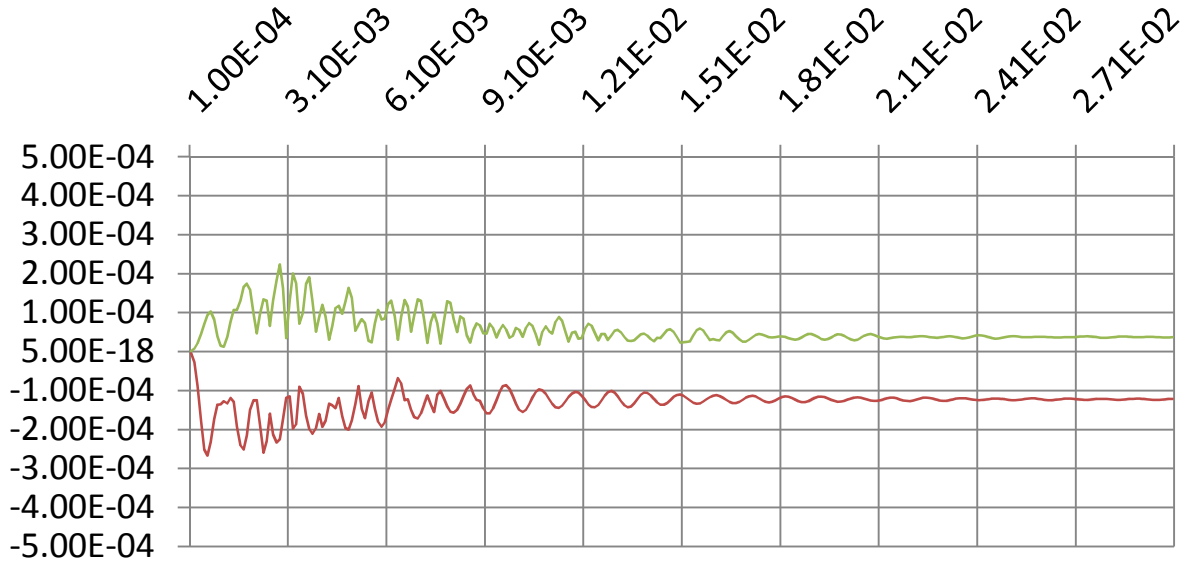

Figure 5.1.2-3 Carriage B-2

When directional deformation data for the carriages A-4 and B-2 are represented in the same plot, directional deformation for the carriage A-4 is barely visible in comparison with the B-2 curve; see figure 5.1.2-4 below.

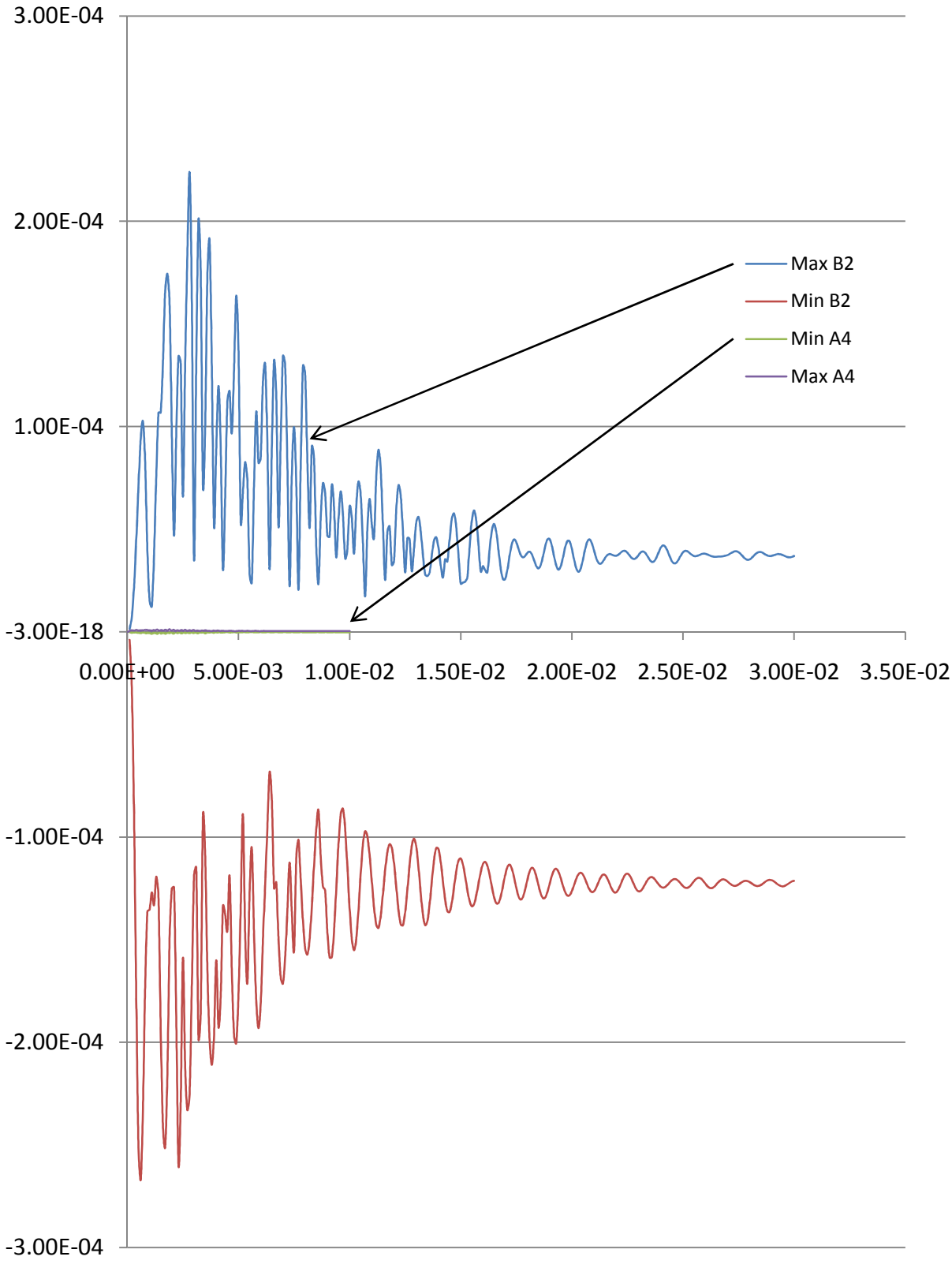

Figure 5.1.2-4 Carriage A-4 and B-2

5.1.3. Results from deformation analysis

Angle deviations of the mirror are calculated with a reflective surface of 130mm length. Angle deviation is represented in terms of milli arc seconds, *mas*. Mirror in the carriage A-4 is much less deformed than in B-1 and B-2. Deviations are three to six times greater during start-up phase compared to steady state. The repeatability of the mirror angular position during operation shall be 1 arcsecond. All structures are within specifications.

	Carriage A-4	Carriage B-1	Carriage B-2
Total static deformation [*nm*]	0.558	165.853	159.360
Angular deviation [*mas*]	0.885	263.151	252.849

Table 5.1.3-1 Angular deviation due to total static deformation

	Carriage A-4	Carriage B-1	Carriage B-2
Total transient deformation [*nm*]	2.15	950	480
Angular deviation [*mas*]	3. 411	1 507.319	761.593
Offset error on sub-reflector [μm]	0.28	122	62

Table 5.1.3-2 Peak angular deviation due to total transient deformation

5.1.4. Modal analysis

A mechanical design's overall mass and stiffness defines the various periods that it will naturally resonate at, the self-resonant frequencies (SRF), (or eigenfrequencies). If a mechanical designs natural frequency's matches the superimposed movement it could continue to resonate and interfere with the function or damage the design. With ANSYS, eigenfrequncies for Carriage A-4, B-1 and B-2 have been simulated; the data presented in Table 5.1.4-1 below.

Nr.	Carriage A-4	Carriage B-1	Carriage B-2
1	618,36	634,44	634,48
2	1166,7	1090,4	966,89
3	1290,8	1163,7	1094,4
4	1867,5	1250,3	1218,1
5	1942,8	1317,2	1243,1
6	2064,2	1832,0	1315,0

Table 5.1.4-1 The first six SRF measured in [Hz] for the carriages.

Choosing the beam switch blanking time 0,1 sec results in a sine wave at 10 Hz. This is well below the first SRF calculated for the carriages above and it can be expected that neither of the designs will be affected by any SRF**.**

5.1.5. Structural stress equivalent (von-Mises)

This simulation shows how the amount of mechanical stress is distributed over the design of the different carriages. Colour variation indicates how the amount of stress varies between locations, red colour (maximum) and blue colour (minimum).

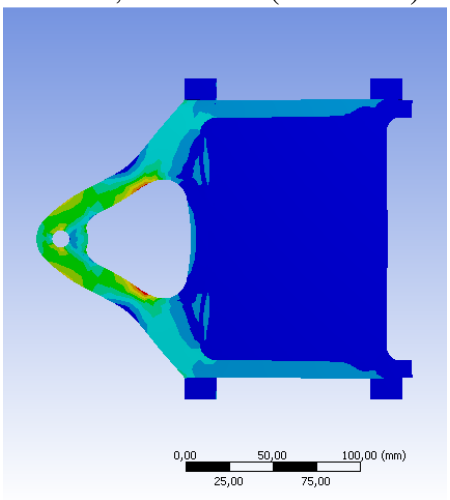

Figure 5.1.5-1 Carriage A-4

Maximum stress
Static: 117.11 kPa
Transient: 230.49 kPa

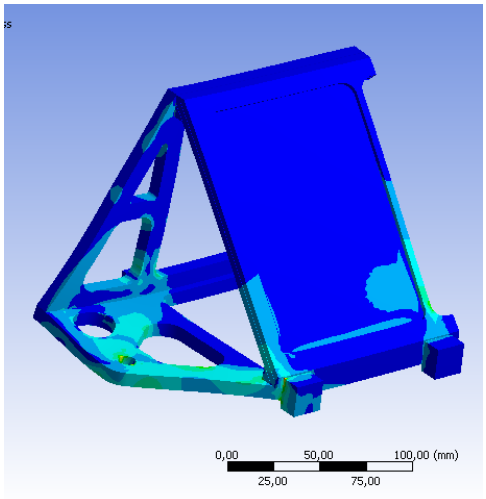

Figure 5.1.5-2 Carriage B-1

Maximum stress
Static: 344.57 kPa
Transient: 681.55 kPa

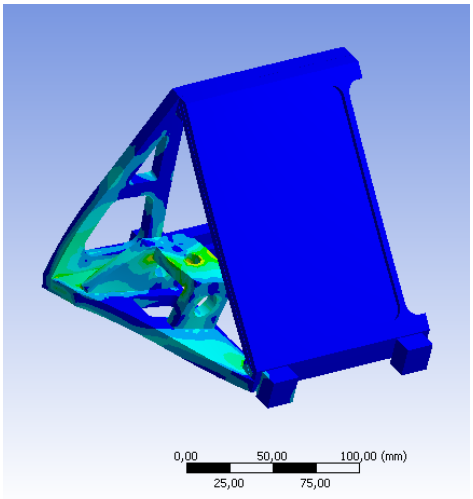

Figure 5.1.5-3 Carriage B-2

Maximum stress
Static: 525.31 kPa
Transient: 1 025.3 kPa

In all designs, the maximum stress occurs in the aluminium frame close to the pulling hole. Aluminium have a Tensile Yield Strength of $280.0 \cdot 10^6$ Pa. Maximum stress is analyzed and predicted in the heaviest design (B-2) pulling hole. Even in this case, it was found to be just $1.0253 \cdot 10^6$ Pa, which is 273 times lower than Tensile Yield Strength for the aluminium alloy.

5.2. Guidance systems, guideway and carriage unit

This is an example to identify, which tolerances are important in a guidance system for the carriages.

5.2.1. Guideways

Critical tolerances of the guideways are to be addressed in this chapter.

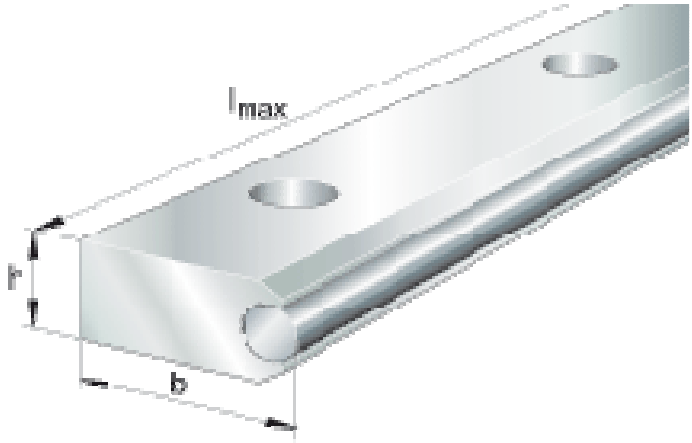

Figure 5.2.1-1 picture of INA guideway LFS 52-FHE, hardened shaft and aluminium rail [10].

In the figure 5.2.1-2, “A” is a parallelism tolerance and “D” is a straightness tolerance. If these are insufficient, then the wheels will slip and wear will occur on the shafts and wheels. This would lead to a backlash in the mirror normal direction and misalignment of the mirror. If the surface (tolerance “C”) is not straight enough, the shaft becomes distorted when it is pulled down to a flat surface. The unparallelism within tolerance “B” along with a width of the guideways of 160mm may cause a misalignment of 103.13 arcsec; however, measurements on similar guidways show higher accuracy. This must be tested and measured in realistic conditions. With the given maximum angular displacement from Chapter 1.4, Requirements, the acceptable backlash would be 0.78µm.

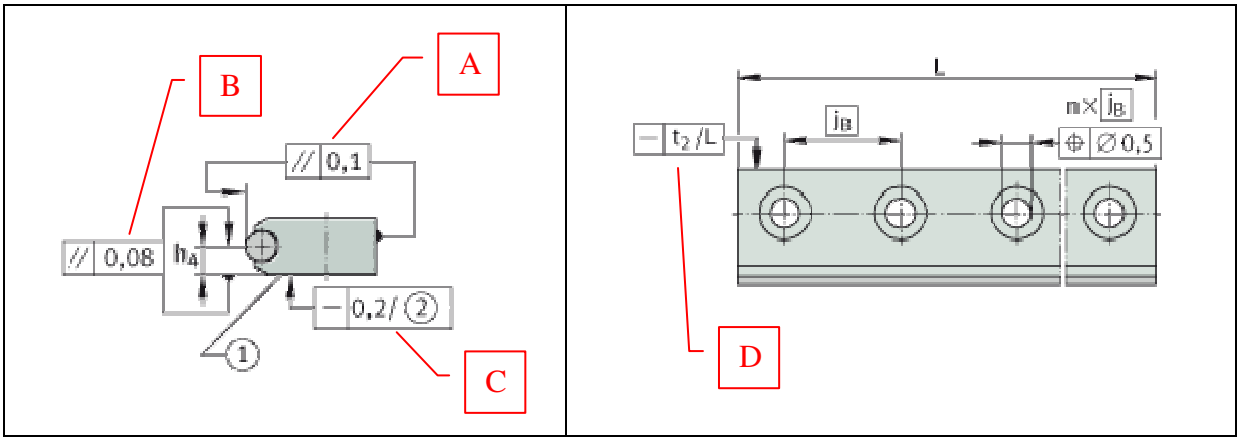

Figure 5.2.1-2 tolerances of the guide ways.

5.2.2. Carriage unit

On the carriage, there were no tolerances specified from vendor (INA). But every µm makes a misalignment of 1.29 arcsec, assuming the width of the guideways is 160mm. Following the chapter 2.1 Angular relations, an angular displacement of the mirror will result in double faults in outgoing beam.

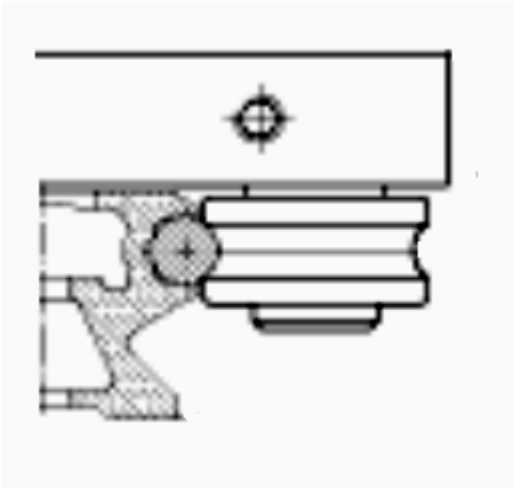

Figure 5.2.2-1 The wheel of carriage LFL52-E-SF from INA.

5.3. Drive unit for sliding mirror beam switch

Various options are possible for the beam switch drive unit. Electric motor is used in beam switches, but there is a risk of high frequency interference from the brush of the motor. Focus will be on pneumatic solutions due to an absence of disturbing electronics. Here, some alternatives are addressed.

5.3.1. Pneumatic actuators

Pneumatic actuators have the advantage that they do not contain any electronics that can cause disturbances to the receiver.

Figure 5.3.1-1 Pneumatic actuators from the RHC series made by SMC [11].

The available force *F*, is calculated for a cylinder with the area *A* and the pressure *P* with the formula (2.5),

An example: *P = 7 bar = 700 kPa, D = 20 mm, D* is the cylinder diameter

$$A = \frac{\pi \cdot D^2}{4} = \frac{\pi \cdot 0.020^2}{4} = 314.159 \cdot 10^{-6}\ [m^2] \quad (5.6)$$

$$F = PA = 700\,000 \cdot 314.159 \cdot 10^{-6} = 219.911\ [N] \quad (5.7)$$

This means that the available force is 220 *N* for the 20 *mm* cylinder. Carriage B-2 is the heaviest of the simulated examples with a weight of 0.716 *kg*. The force needed to accelerate it to 30 m/s^2 is calculated with equation (2.4)

$$F = ma = 0.716 \cdot 30 = 21.48\ [N] \quad (5.8)$$

The pneumatic actuator provides the force, which is more than enough to drive the carriage.

One thing to take in consideration is the life expectancy of pneumatic actuators. Life expectancy is measured in distance travelled by the actuator. But there are various factors involved. Important factors that affect are for instance supply pressure and temperature. It is also heavily dependent on the air quality, and especially on water content. The moist in the air may condense in the actuator and washes out lubricant in the pre-lubricated actuator. There are two solutions to this problem.

The first solution is to use a refrigerated air dryer to remove moisture from the compressed air by cooling the air to a temperature that causes the moisture in the air to condense. Water is now separated from the air stream and can then be discharged from the dryer.

The second solution is to use continuous oil mist lubrication. In the long run, this is a better solution, however, once begun, the oil mist lubrication cannot be discontinued.

Velocity is also a limitation for many pneumatic actuators in both acceleration $[m/s^2]$ and velocity $[m/s]$. Deceleration of the total mass must also be at an appropriate level for the actuator. Important external factors that affect the actuator are things that concern flow rate which in turn affect the pressure such as valves, hose diameter, angled nipples, and if quick exhaust valves are used [12]. One solution is to use a linkage system with a loss of force, but gain in speed, nevertheless this makes it more complex with more parts and bearing joints.

5.3.2. Crankshaft mechanism

Another alternative to the sliding mirror drive could be a crankshaft mechanism. It has the advantage of even and smooth motion with a relatively sleek change in direction. There are pneumatic motors, if electric motors cannot be used. The ability to have a cycle time shorter than 1 second is probably more likely with this solution. The drawback is that the wheel will be quite large due to short blanking time, specified to maximum one-tenth of the cycle.

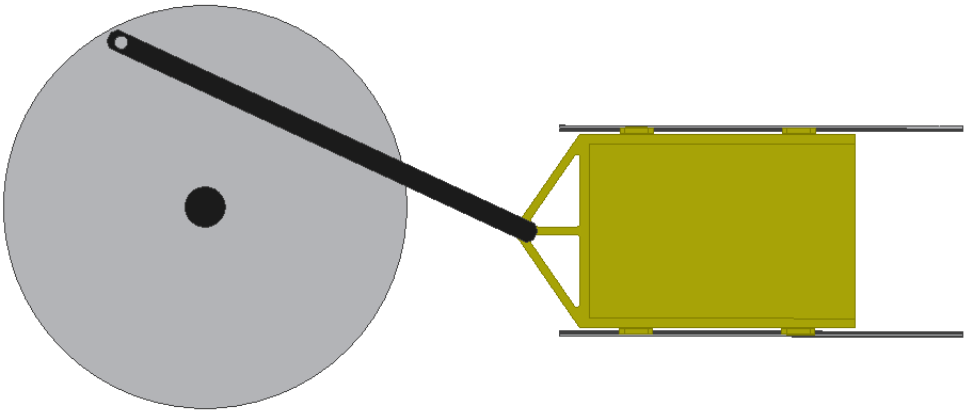

Figure 5.3.2-1 schematic picture of crankshaft mechanism and mirror with guide ways.

The blanking time should not be more than one-tenth of a complete revolution, which means that it must be performed on one-tenth of 360 degrees which is 36 degrees. This leads to a wheel of 260mm in diameter for a beam with the diameter of 80mm (5x beam radius) as shown in Figure 5.3.2-2.

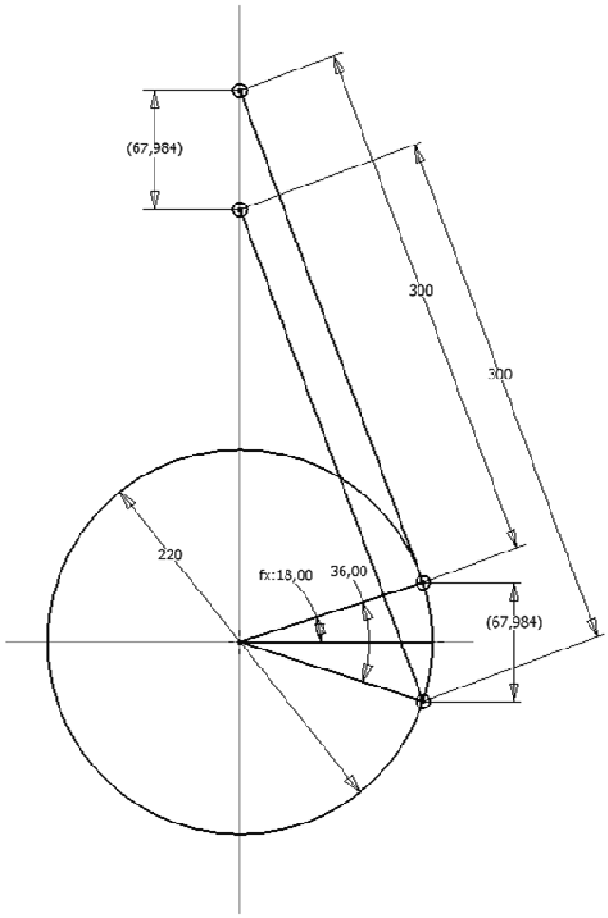

Figure 5.3.2-2 Determination of the rotation diameter in Autodesk Inventor

A space-saving option could be a use of elliptical wheels to drive the mirror. The motor driving the first wheel has constant speed but the elliptical shape causes variation in rotating speed on the second wheel. This offers the possibility of relatively long times at the end positions, where the mirror moves at a lower speed, and quick movement in the transition between on/off-source.

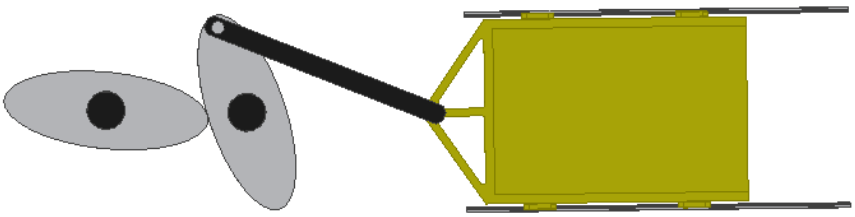

Figure 5.3.2-3 schematic picture of the elliptical wheel solution

CHAPTER 6

CONCLUSIONS

Five different switching methods have been evaluated and one of them has been analyzed in detail. A 3D model has been made in the CAD system Autodesk Inventor and mechanical analysis in the FEM software ANSYS. The analysis includes static structural directional deformation during acceleration, transient structural directional deformation during acceleration, modal analysis and static structural stress equivalent (von-Mises). Different mechanical drives have been evaluated and partly analyzed.

- Simulation in ANSYS shows that there are very low levels of deformation and vibration in the direction normal to the mirror's surface due to acceleration. The carriage A-4 had a maximum total static deformation, which resulted in an angular error of 0.885 *mas* and total transient deformation of 3. 411 *mas*. Carriage B-2, the better of the two larger designs had a maximum total static deformation of 252.849 *mas* and total transient deformation of 761.593 *mas*. This is better than the 1 arc second specified as requirements. Even if carriage B-2 has relatively low levels of deformation, it cannot be recommended due to its additional mechanical complexity.

- Modal analysis has shown that the carriage A-4 had lowest SRF, which has the first SRF at 618.36 Hz. The 10 Hz excitation from mirror switching is well below this first SRF.

- Carriage B-2 had th**e** highest Structural stress of 1.025 MPa, which is still 273 times lower than Tensile Yield Strength for the aluminium alloy of 280.0 MPa.

- The guideways manufacture tolerance is not sufficient, but measurements on similar guideways show higher accuracy. This needs further testing in realistic conditions.

- Driving the carriage with a pneumatic actuator has uncertainties in speed and lifetime which need to be investigated. A crankshaft mechanism will have a smoother and more stable motion, but occupies more space. Elliptical wheels are maybe a solution to reduce the required space and it, in addition, offers the possibility to have variable speed of the motion with the highest speed during the transition part and lower speed during change of direction.

CHAPTER 7

SUGGESTIONS FOR FUTURE WORK

Future research should be done with focus on drive unit and guideways. Because the speed is at the limit of what a pneumatic actuator can provide, a practical testing is needed. More studies regarding the guideways are necessary. A study with experiments and observations should give the answers. The reason for this is that all practical details are hard to simulate in software.

- Find out the risk of using electric motors in the receiver cabin. What can cause interfere with the receiver, does an electric brushed motor generate disturbing frequencies, is the magnetic field from an electric motor any problem, does the driving unit to a brushless motor disturb the receiver and is it possible to use a servo motor are some of the questions that need to be answered. Where is the limit? Interference vs. mirror positioning accuracy.

- Are there other areas/industries where mirrors are used in a similar ways? How do they do it?

- For the sliding mirror solution. Assemble and test the guideways. Are they stable enough? Investigate what happens at high speed and acceleration? Is it possible to get them parallel enough?

- Investigate if the pneumatic actuator can provide sufficient speed. A mass equivalent to the mass of the carriage should be installed on the piston rod. Vibrations due to accelerations and deceleration should be measured.

List of Abbreviations

CAD	Computer-Aided Design
FEM	Finite Element Method
GARD	Group for Advanced Receiver Development
mas	milli arc seconds
OSO	Onsala Space Observatory
PCB	Printed Circuit Board
SRF	Self-Resonant Frequency

References

1. GARD web site, http://www.chalmers.se/rss/EN/research/research-groups/advanced-receiver (2011-01-31).
2. Onsala Space Observatory official web site, http://www.chalmers.se/rss/oso-en/ (2011-01-31).
3. Grahn, R., Jansson, P., (2002) Mekanik - statik och dynamik. Lund: Studentlitteratur.
4. Çengel, Yunus A., (2008) *Fundamentals of thermal-fluid sciences,* Third edition in si units, New York [United States]: McGraw Hill Higher Education.
5. Bureau international des poids et mesures (BIPM) web site, Système International d'Unités, The SI-system, http://www.bipm.org/en/CGPM/db/11/12/ (2011-01-24).
6. Inventor, 3D mechanical solid modeling design software from Autodesk. http://www.autodesk.se/adsk/servlet/pc/index?id=14569091&siteID=440386 (2011-02-16)
7. ANSYS simulation software from ANSYS Inc, www.ansys.com . (2011-01-31)
8. Per Björklund, Onsala Space Observatory, Onsala, Tel: +46 (0)31 772 55 69
9. http://en.wikipedia.org/wiki/FR-4 (2011-02-15)
10. INA web site, http://www.ina.com (2011-02-15)
11. SMC web site, http://content.smcetech.com/pdf/RHC_EU.pdf (2011-01-25)
12. Tommy Boström, Norgren Sweden AB, Malmö, Tel: +46 (0)40 595176

APPENDIX A, technical data.

	Carriage		
	A-4	**B-1**	**B-2**
Mass [kg]	0.338	0.642	0.716

Table A-1 Carriage mass

Material properties used in ANSYS simulations			
Mechanical properties	Mirror	Frame	Wheels
Material	FR-4	Aluminium alloy	Structural steel
Density [kg/m^3)	1904.7	2770	7850
Young's Modulus [Pa]	17.0 $\cdot 10^9$	71.0 $\cdot 10^9$	200.0 $\cdot 10^9$
Bulk Modulus [Pa]	7.784 $\cdot 10^9$	69.608 $\cdot 10^9$	166.667 $\cdot 10^9$
Shear Modulus [Pa]	7.482 $\cdot 10^9$	26.692 $\cdot 10^9$	76.923 $\cdot 10^9$
Tensile Yield Strength [Pa]	344.738 $\cdot 10^6$	280.0 $\cdot 10^6$	250.0 $\cdot 10^6$
Compressive Ultimate Strength [Pa]	413.685 $\cdot 10^6$	310.0 $\cdot 10^6$	460.0 $\cdot 10^6$

Table A-2 Material properties

APPENDIX B, drawings

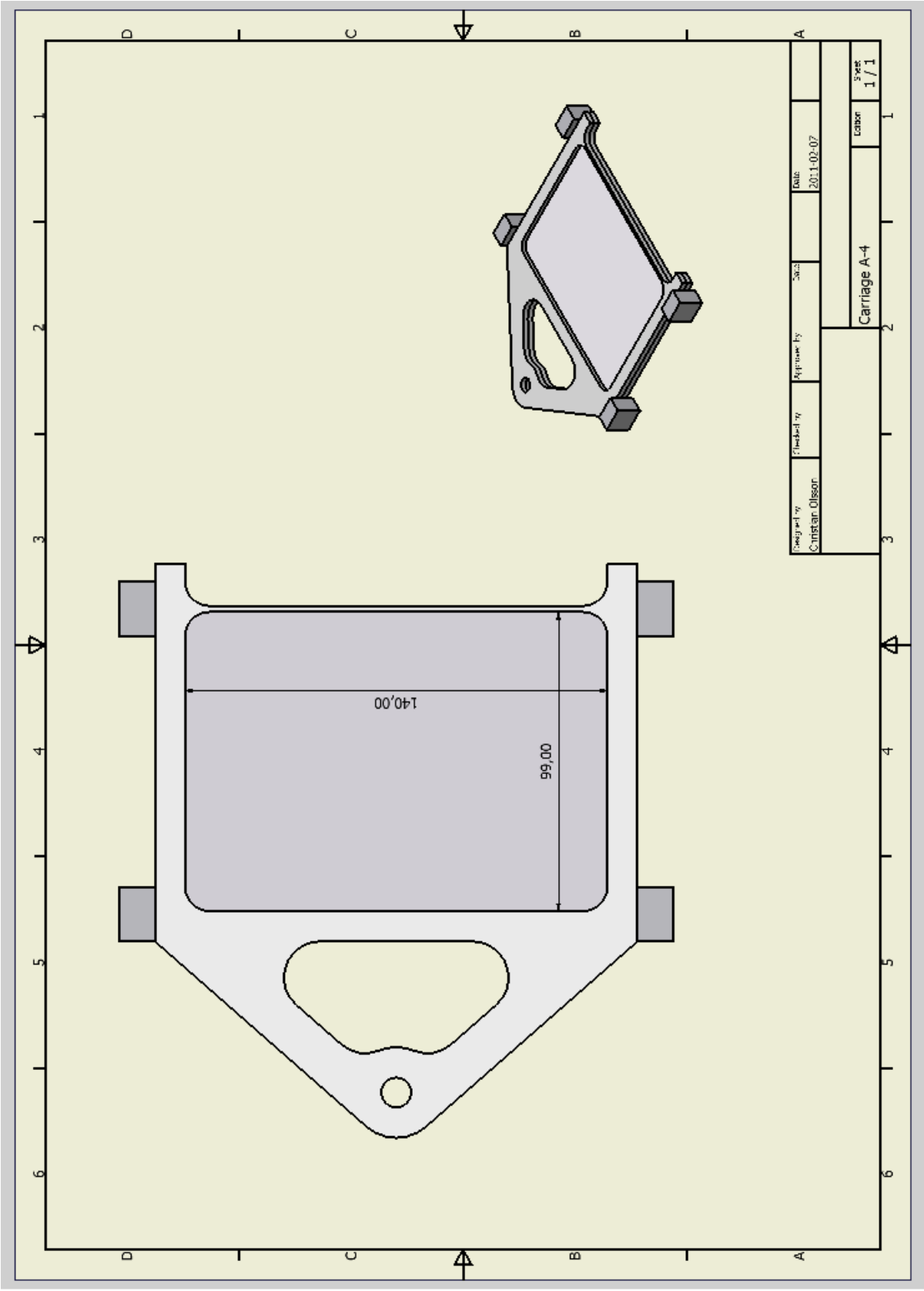

Drawing B-1 Carriage A-4

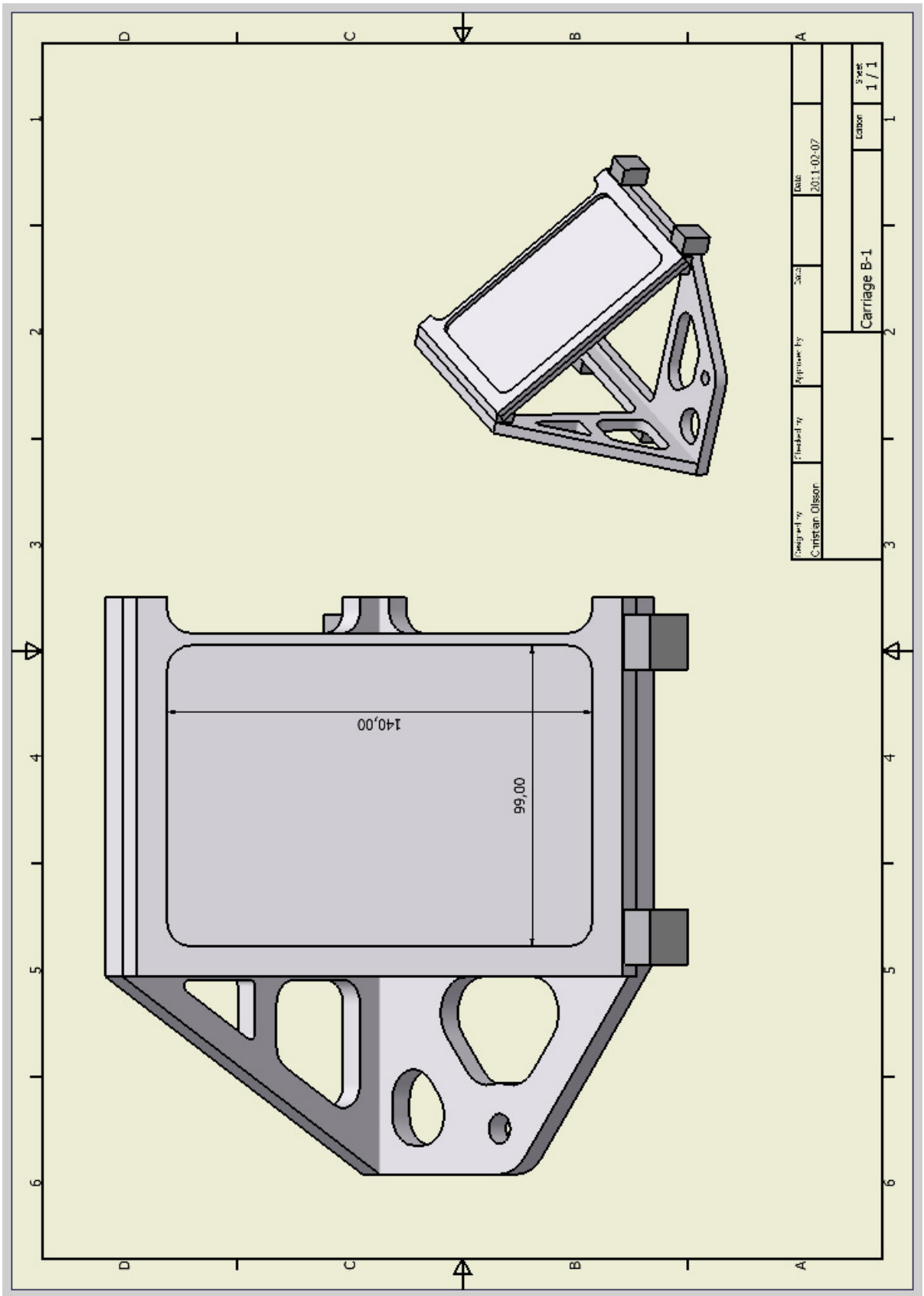

Drawing B-2 Carriage B-1

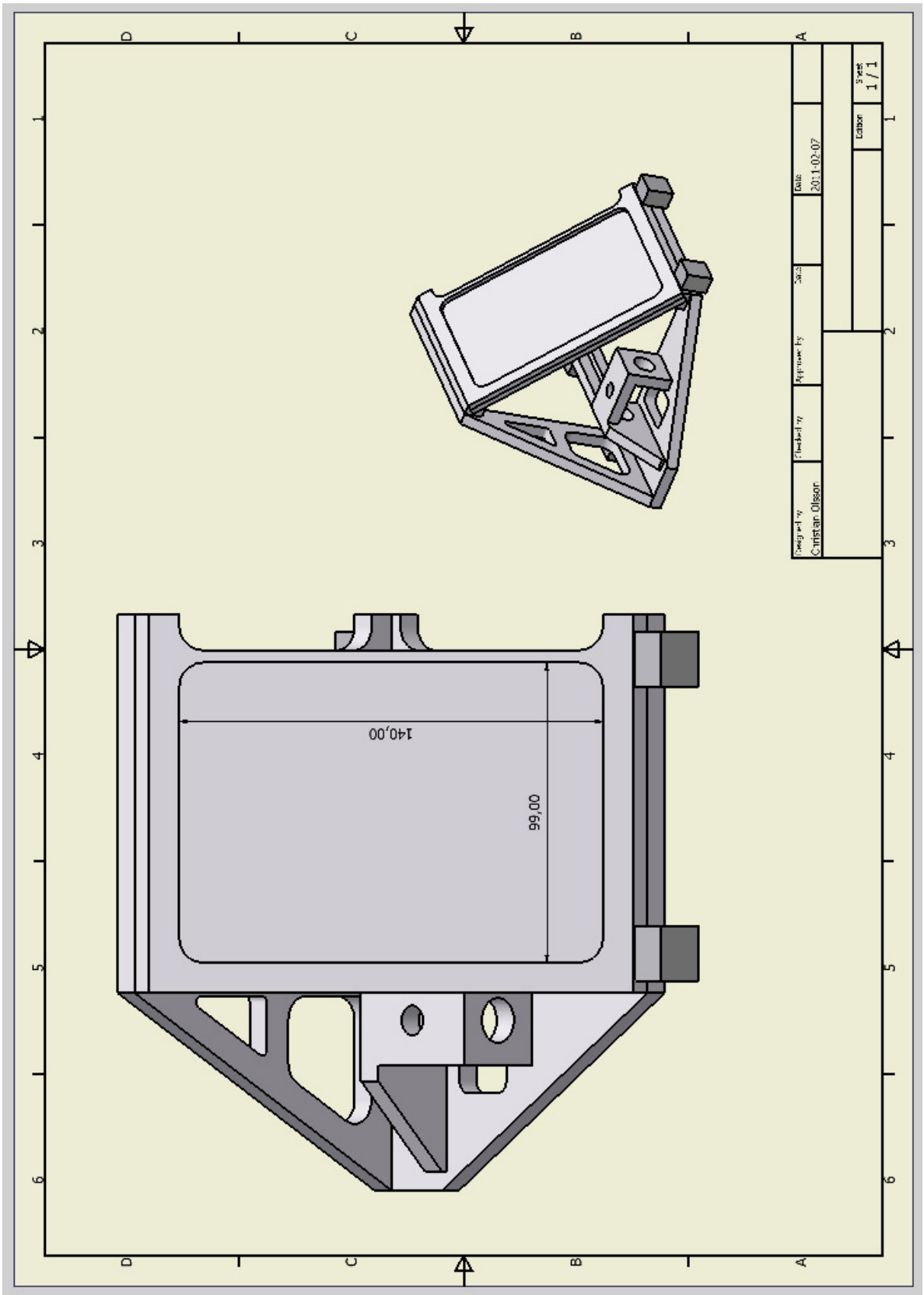

Drawing B-3 Carriage B-2